Environmental Science
Water Research & Technology

ROYAL SOCIETY OF CHEMISTRY

PAPER

View Article Online
View Journal | View Issue

Cite this: *Environ. Sci.: Water Res. Technol.*, 2025, **11**, 2555

Valorization of waste-derived coffee husk into a sustainable adsorbent for multicomponent pharmaceutical removal from complex wastewater under continuous-flow conditions

Valentina Ospina-Montoya,[a] Samuel Aguirre-Contreras,[c] Raúl Ocampo-Pérez,[c] Erika Padilla-Ortega,[c] Sebastián Pérez,[d] Juan Muñoz-Saldaña,[d] Jazmín Porras,*[b] Nancy Acelas*[a] and Angélica Forgionny *[a]

This study elucidates the competitive adsorption dynamics of ciprofloxacin (CIP) and acetaminophen (ACE) onto coffee husk activated with potassium (CH–KOH, BET surface area = 1145 m^2 g^{-1}, pH_{PZC} = 7.36), providing mechanistic insights into the removal of pharmaceuticals in complex aqueous matrices. The Modified Langmuir multicomponent isotherm effectively captured the competitive equilibrium behavior (deviation = 25.8%), showing a higher affinity for ACE (η_{ACE} = 0.7) than for CIP (η_{CIP} = 4.9), the qT was 1.25 mmol g^{-1} across the entire evaluated concentration range, which is similar to the observed in mono-component systems, Q_{max} 1.26 mmol g^{-1} for ACE and 0.58 mmol g^{-1} for CIP, with removal efficiencies of 91–99% and 75–99%, respectively. In real matrices such as synthetic hospital wastewater and urine, high efficiencies (84–97%) were maintained. Fixed-bed column studies confirmed the strong performance under continuous-flow conditions, with saturation capacities (q_s) up to 1.46 mmol g^{-1} for ACE and 0.61 mmol g^{-1} for CIP, mass transfer zones ranging from 0.42 to 1.53 cm, and breakthrough times between 91 and 1463 min depending on flow rate (1–3 mL min^{-1}) and bed height (1–3 cm). The Thomas model accurately predicted breakthrough curves, revealing faster kinetics for ACE. Physisorption predominates, involving synergistic π–π stacking interactions, hydrogen bonding networks, and hydrophobic association, with ACE showing greater selectivity in both mono and multicomponent systems. CH–KOH exhibited high stability and reusability, stabilizing at approximately 70% of its initial capacity by the third cycle, with no further decrease observed in the fourth cycle. Comprehensive physicochemical characterization revealed that physisorption predominates, involving synergistic π–π stacking interactions, hydrogen bonding networks, and hydrophobic associations. These results confirm the potential of CH–KOH as a sustainable adsorbent for pharmaceutical contaminant removal in real-world scenarios, integrating circular economy principles into advanced water treatment.

Received 31st May 2025,
Accepted 10th September 2025

DOI: 10.1039/d5ew00499c

rsc.li/es-water

Water impact

This study valorizes coffee husk waste into an efficient adsorbent for removing pharmaceuticals from complex wastewater. By demonstrating high performance in continuous-flow systems and realistic matrices (synthetic hospital wastewater and urine), the work highlights a scalable circular economy solution for sustainable water treatment.

1. Introduction

Emerging pollutants (EPs) are substances detected in the environment that pose potential risks to human health and ecosystems.[1] Despite their potential hazards, many EPs remain unregulated in several countries.[2] While EPs have been released into the environment for decades, their detection has only recently become feasible due to advancements in analytical techniques.[3] Among these contaminants, pharmaceutical compounds including hormones, anti-inflammatory drugs, antibiotics, and

[a] *Grupo de investigación Materiales con Impacto (Mat&mpac), Facultad de ingenierías, Instituto de Ciencias Básicas, Universidad de Medellín, Carrera 87 No. 30-65, Medellín 050026, Colombia. E-mail: nyacelas@udemedellin.edu.co, mforgionny@udemedellin.edu.co; Tel: +57(604) 5904500*
[b] *Grupo de Investigaciones Biomédicas UniRemington, Corporación Universitaria Remington, Calle 51 No. 51-27, Medellín 050010, Colombia. E-mail: jazmin.porras@uniremington.edu.co; Tel: +57(604)3221000*
[c] *Centro de Investigación y Estudios de Posgrado, Facultad de Ciencias Químicas, Universidad Autónoma de San Luis Potosí, San Luis Potosí, 78260, Mexico*
[d] *Centro de Investigación y de Estudios Avanzados del Instituto Politecnico Nacional, Laboratorio Nacional de Proyección Térmica (CENAPROT), Libramiento Norponiente 2000 Fracc, Real de Juriquilla, 76230, Querétaro, Mexico*

antidepressants are of particular concern due to their persistence and widespread presence in aquatic systems. These substances enter water bodies through wastewater discharges, agricultural runoff, and inadequate treatment processes.[4] Studies have confirmed the presence of these substances in rivers, lakes, groundwater, and even oceans, often at trace concentrations (ng L^{-1} to μg L^{-1}).[5–8] Despite their low levels, these pollutants can induce endocrine disruption, antibiotic resistance, bioaccumulation, and ecological imbalances in aquatic communities.[5,9] The increasing consumption of pharmaceuticals, driven by population growth and economic development, further exacerbates their environmental release.[3,10]

Acetaminophen (ACE) and ciprofloxacin (CIP) exemplify the challenges posed by EPs in wastewater systems. ACE, a commonly consumed analgesic, is often detected in effluents, with 58–68% of ingested doses excreted unchanged in urine.[11] While ACE is moderately toxic to aquatic organisms, its degradation byproducts (*e.g.*, 4-aminophenol) are mutagenic and carcinogenic.[12] CIP, a fluoroquinolone antibiotic that poses additional risks, including toxicity to aquatic life and the promotion of antibiotic-resistant bacteria.[13] Despite these threats, regulatory frameworks for controlling their discharge remain inadequate in many regions.

Conventional wastewater treatment plants (WWTPs), which primarily rely on physical and biological processes, are not specifically designed to eliminate micropollutants such as pharmaceuticals. These compounds often exhibit low biodegradability and strong stability under standard treatment conditions, leading to incomplete removal. In some cases, effluent concentrations of certain drugs have been reported to be higher than influent levels. This may be due to the desorption of compounds from sludge, biotransformation of conjugates back to the parent drug, or analytical matrix suppression in influents. Such behavior has been observed in various studies, Botero-Coy *et al.* (2018).[14–18] Advanced technologies, such as electrocoagulation,[19] sonochemical treatment,[20] biological treatment,[20] advanced oxidation,[21] membrane filtration processes,[22,23] and photocatalytic degradation[24] have shown promise, but their high energy demands, operational costs, and secondary waste generation limit scalability. In contrast, adsorption using activated carbon is a cost-effective, efficient alternative that leverages its high surface area, porosity, and chemical stability.[25–29]

Current research on removing pharmaceuticals from wastewater predominantly focuses on mono-component batch systems, failing to address the competitive adsorption dynamics characteristic of real wastewater matrices. Comprehensive multicomponent analyses and continuous-flow experiments are essential to bridge this critical knowledge gap for optimizing operational parameters in practical applications. Selecting appropriate adsorbent materials is another crucial consideration in this field. Although activated carbon has excellent adsorption capacity, its high production costs and disposal challenges significantly limit large-scale implementation.[30]

In response to these limitations, agro-industrial waste materials have emerged as sustainable and low-cost alternatives for producing biochar and activated carbon with optimal adsorption properties. Numerous studies have demonstrated the effectiveness of various agricultural byproducts for this purpose, including sugar cane bagasse,[31] coffee waste,[32] spent tea leaves,[33] grass,[34] beer grains,[35] avocado seeds,[36] bamboo chips,[37] cellulose factory sludge[38] in removing pharmaceutical compounds.

Chemical activation processes using agents such as phosphoric acid, potassium hydroxide (KOH) or zinc chloride significantly enhance the porosity and pore volume structure of these materials. Among these activating agents, KOH has proven particularly effective, consistently producing adsorbents with well-defined pore structures, a high specific surface area and favorable yields.[31,33,35,37]

Recent investigations have confirmed the exceptional performance of KOH-activated agricultural waste-derived carbons in removing EPs, positioning them as promising sustainable solutions for advanced wastewater treatment.[39–42]

Egbedina *et al.* (2021)[65] prepared KOH-activated coconut husk–kaolinite biochar *via* a microwave technique, achieving a Q_{max} 229 mg g^{-1} for CIP in batch mode. Liu *et al.* (2023)[66] reported activated carbon from waste peony seed shells with an ultra-high specific surface area (2980.96 m^2 g^{-1}) and CIP removal (Q_{max} = 782.3 mg g^{-1}). In contrast, Li *et al.* (2018)[67] obtained potato stem–leaf biochar (38.75 m^2 g^{-1}) activated with KOH, which reached 23.36 mg g^{-1} for CIP removal. In these cases, adsorption mechanisms included hydrophobic interactions, hydrogen bonding, electrostatic attraction, and π–π interactions.

The accumulation of environmental impact of agro-industrial waste presents a particularly pressing challenge, in coffee-producing nations like Colombia. As the world's third-largest coffee producer after Brazil and Vietnam, Colombia harvested 820 600 tons of coffee from 839 700 hectares in recent years, generating substantial waste volumes.[43,44] The coffee processing chain remains remarkable inefficient, generating waste that ranges from 30% to 50% of the total weight of coffee processed.[45] Specifically, processing one ton of fresh coffee cherries yields approximately 0.5 tons of pulp and 0.18 tons of husk.[46] Currently, these residues lack economically viable applications and often accumulate in landfills, creating serious environmental concerns.[46,47] The high lignin content (21%) and slow degradation rates of coffee processing byproducts exacerbate these issues, leading to methane emissions and other negative environmental impacts when they accumulate in stockyards and dumpsites.[48,49] Converting coffee husks into value-added adsorbent materials offers a dual solution by simultaneously addressing waste management challenges in the coffee industry and providing sustainable water

treatment options that align with circular economy principles.

This study aims to advance understanding of the adsorption process of ciprofloxacin and acetaminophen adsorption onto KOH-activated coffee husk-derived carbon through a comprehensive experimental approach.

Therefore, this work focuses on exploring the adsorption behavior of these compounds in greater detail using various experimental techniques. The methodology progresses systematically from fundamental batch experiments to practical applications, beginning with mono-component isotherm studies to establish baseline adsorption characteristics. Interactions between the adsorbent and contaminants were analyzed using advanced spectroscopic techniques, including Fourier transform infrared spectroscopy (FTIR) and X-ray photoelectron spectroscopy (XPS). The investigation then advances to more realistic scenarios through multicomponent analysis and continuous-flow fixed-bed column experiments specifically targeting CIP and ACE removal. Additionally, the adsorbent's recyclability was evaluated alongside its performance in complex matrices such as synthetic wastewater and urine—an approach rarely reported for agricultural waste-derived carbons to assess practical feasibility. By integrating fundamental adsorption studies with fixed-bed continuous-flow evaluations under realistic water matrices, this work bridges the gap between lab-scale testing and real-world application, providing critical insights for developing improved contaminant removal strategies in complex wastewater systems.

2. Materials and methods

2.1. Raw material

Coffee husk waste was collected from coffee bean processing operations in Santa Bárbara, Antioquia, Colombia. The raw material underwent thorough washing with deionized water to remove surface impurities, followed by drying at 100 °C for 24 h in a convection oven (Memmert model). The dried husk was sieved to obtain particles with an uniform size distribution (average diameter 450 μm) and stored as "CH", (coffee husk) for subsequent.

2.2. Adsorbent synthesis

Coffee husk activated with potassium hydroxide (CH–KOH) was prepared *via* a one-step thermochemical activation process using KOH (≥85% purity, PanReac AppliChem) at a 1 : 1 mass ratio in 30 mL of deionized water, stirred at room temperature at 300 rpm for 2 h and aged for 12 h.[39,50] The slurry was oven-dried at 105 °C for 12 h before pyrolysis in a horizontal tube furnace with three temperature-controlled zones (model OTP-01, Resistencias y Equipos, Colombia), heated from room temperature to 700 °C at a rate of 5 °C min^{-1} and held for 1 h under a N_2 flow of 100 mL min^{-1}. Post-processing involved washing the activated material with 30 mL of 2 M HCl solution under continuous stirring at 300 rpm for 3 h. The sample was then extensively rinsed with deionized water to achieve a neutral pH, ensuring the removal of residual inorganic compounds and activating agents. Finally, the solid was dried at 105 °C for 12 h, stored, and labeled as CH-KOH.

2.3. Physicochemical characterization of activated carbon

The physicochemical properties of CH–KOH were determined using various techniques. Textural properties were evaluated using N_2 adsorption–desorption isotherms collected at −196 °C using an ASAP 2020 analyzer (Micromeritics Instrument Corporation, USA). Before analysis, the CH–KOH was degassed at 100 °C under vacuum (10^{-2} Pa) for 12 h. The surface area was determined using the Brunauer–Emmett–Teller (BET) method,[51] and complemented by total pore volume (TPV) and average pore diameter (APD) measurements.[52] Boehm titrations were conducted using a standardized procedure to quantify the acidic groups present on the adsorbent surface.[53] The pH at point of zero charge (pH_{PZC}) was determined *via* the solid addition method, in accordance with eqn (S1)–(S5).[54]

The surface functional groups were characterized using Fourier transform infrared spectroscopy with attenuated total reflectance (ATR-FTIR) accessory, scanning the spectral range of 4000 to 450 cm^{-1} with a Spectrum Two spectrometer (PerkinElmer, Waltham, Massachusetts, USA). The phase structure of CH–KOH was analyzed using X-ray diffraction (XRD) with a Rigaku SmartLab diffractometer operating at 44 kV and 40 mA and equipped with a Cu $K\alpha_1$ radiation source (λ = 1.5406 Å) both before and after adsorption. Diffraction patterns were recorded over a 2θ range of 10° to 70°, with a step size of 0.02° and a scan rate of 5° min^{-1}. The microstructure of CH–KOH, before and after adsorption was characterized using a JSM-7610F scanning electron microscope (SEM, JEOL) operating at an acceleration voltage of 15 kV, utilizing a secondary electron detector for imaging.

The surface chemical composition and oxidation states of CH–KOH, before and after adsorption were analyzed using X-ray photoelectron spectroscopy (XPS). Spectra were recorded using a Scanning XPS micro – probe PHI 5000 VersaProbe II, with an Al K X-ray source ($h\nu$ = 1486.6 eV) monochromatic with a 100 μm beam diameter, and an MCD analyzer. The binding energy (BE) scale was calibrated by setting the C1s peak at 284.8 eV. Spectral deconvolution was performed by curve fitting following Shirley-type background subtraction and asymmetric functions were considered with a line shape SGL(p)T(k) utilizing the CasaXPS software.[55]

2.4. Adsorption experiments

2.4.1. Preliminary test. Batch adsorption experiments were performed to compare the adsorption efficiency of CH–KOH material. For each experiment, 50 mg of adsorbent was added to 100 mL of aqueous solutions containing either CIP or ACE at initial concentrations of 200 mg L^{-1}. The suspensions were agitated at 200 rpm for 180 min to ensure proper contact between the adsorbent and the target contaminants. The

removal percentage (%R) and time-dependent adsorption capacity (q_t) were calculated using eqn (S6) and (S7), respectively.

2.4.2. Effect of solution pH. The pH-dependent adsorption behavior was also examined across a pH range of 2 to 10. The solution pH was carefully adjusted and maintained using standardized HCl and NaOH solutions at concentrations of 0.01, 0.1, and 1.0 M. All experimental suspensions were kept under continuous agitation at 200 rpm for 180 min to ensure thorough interaction between the adsorbent and the pharmaceutical compounds.

2.4.3. Equilibrium adsorption experiments in mono-component system. Individual adsorption isotherms were determined using CIP and ACE solutions from 0.060 to 0.241 mmol L^{-1} initial concentrations. The experiments were carried out by contacting 0.0125 g of adsorbent with a volume of 100 mL of each contaminant solution at pH 6. The suspensions were kept under constant stirring at 200 rpm for 3 h in an orbital shaker (Actum, HD300). The experimental equilibrium data were analyzed using the Langmuir (eqn (S8)) and Freundlich (eqn (S9)) isotherm models.[56]

2.4.4. Equilibrium adsorption experiments in multicomponent system. In multicomponent systems, the experiments were carried out by contacting 0.0125 g of adsorbent with a volume of 100 mL of each contaminant solution at pH 6. The suspensions were kept under constant stirring at 200 rpm for 3 h in an orbital shaker (Actum, HD300). The experimental equilibrium data were analyzed using the Langmuir (eqn (S8)) and Freundlich (eqn (S9)) isotherm models.[56] A 6 × 6 matrix was created by varying the concentrations of ACE and CIP (see Table S2 in the SI material). All experiments were conducted at pH 6, controlled using 0.01 N NaOH and 0.01 N HCl solutions until equilibrium was reached. The ionic strength (0.01 N) was maintained constant throughout the experiments. The binary adsorption tests were carried out in batch mode under the same conditions as the individual adsorption experiments. The concentrations in the binary system ranged from 0.060 to 0.241 mmol L^{-1}. The initial and final concentrations of both pharmaceuticals were measured using high-performance liquid chromatography (HPLC) with a Thermo Scientific Dionex Ultimate 3000 UHPLC system. The experimental data of CIP and ACE in a multicomponent system on CH–KOH were analyzed at equilibrium conditions by the Langmuir multicomponent: the extended Langmuir model (LME) and the modified Langmuir multicomponent isotherm (MLMη_i) with an interaction factor η_i (eqn (S10) and (S11), respectively).[57] The LME model assumes that the adsorption sites are energetically identical, with species in solution competing for the same available sites. The isotherm parameters are determined by fitting the multicomponent adsorption equilibrium data of each species to the LME isotherm.[58] The MLMη_i model is based on the individual Langmuir isotherm. Therefore, it uses the individual isotherm parameters while incorporating an interaction factor to account for the competitive adsorption of species. This factor is characteristic of each species and depends on the concentrations of other components in the solution. The interaction factor can be estimated from competitive adsorption equilibrium data. In the MLMη_i model, the interaction factor denoted by η_i plays a key role. The phenomenon is associated with the component i's affinity for the adsorbent. In a multicomponent system, the affinity of component i for the adsorbent decreases as the value of η_i increases. This indicates that the higher the value of η_i, the lower the affinity of component i for the adsorbent in a competitive adsorption environment.[59]

2.4.5. Column adsorption experiments. Fixed-bed adsorption tests for ACE and CIP were conducted using a glass tube with an internal diameter of 1.1 cm and height of 15 cm. Breakthrough curves (C/C_0 *versus* time) were obtained at 25 °C. The column was loaded with a known mass of CH–KOH, with alumina spheres placed at both ends to ensure bed compaction and minimize dead volume and channeling effects. The height of the filler layer in fixed-bed adsorption columns was set at 1 cm, 2 cm, and 3 cm, while the flow rate of the feed solution was set at 1 mL min^{-1}, 2 mL min^{-1}, and 3 mL min^{-1}. For the adsorption test, three different concentrations of each contaminant (CIP or ACE) aqueous solution, namely 0.093, 0.121, 0.152 mmol L^{-1} were utilized.

The contaminant solutions were introduced using a peristaltic pump (SHENCHEN LabV6-111) at controlled flow rates. Contaminant concentrations were measured at various time intervals from the beginning of the experiment until column saturation (C/C_0 = 1 or constant), and the breakthrough curves were plotted. A series of characteristics of the adsorbent in the continuous flow column were determined using breakthrough curves. These characteristics included saturation time (t_s), breakthrough time (t_b), mass transfer zone (MTZ), the adsorption capacity of the column at the breakthrough time (q_b), and adsorption capacity of the column at the saturation time (q_s) calculated using eqn (S12) and (S13). The experimental rupture curves were fitted to two common models for interpretation, represented by Thomas[60] (eqn (S14)) and Clark[61] (eqn (S15)).

2.4.6. Environmental matrix studies and reuse cycles. The adsorption performance in complex matrices was evaluated using hospital wastewater and synthetic urine (see Table S3 for composition details). The experiments involved the addition of CIP or ACE (0.06 and 0.01 mmol L^{-1}, respectively) to 200 mL of each matrix, followed by contact with 25 mg of CH–KOH. The suspensions were maintained under constant agitation at 200 rpm for 300 minutes.

The reusability of CH–KOH was assessed through four consecutive adsorption–desorption cycles. The adsorbent was recovered by vacuum filtration after adsorption and then regenerated *via* ultrasonic treatment (Digital Pro, PS-30AL) at 40 KHz for 30 min in a solution containing 33.3 mL methanol and 6.6 mL of 3% NaOH solution. The regenerated material was then vacuum washed with 700 mL deionized water and dried at 100 °C for 24 h.

3. Results and discussion

The adsorption performance of CH and thermochemically activated CH–KOH was evaluated for the removal of CIP and ACE. Untreated CH showed selective adsorption of CIP, while ACE was not significantly adsorbed due to its neutral character and the limited porosity of the raw material. In contrast, CH–KOH exhibited a remarkable increase in adsorption efficiency for both contaminants. This enhancement is attributed to increased surface area (1145 m^2 g^{-1}), micropore development, and the enrichment of oxygenated functional groups introduced by KOH activation.

3.1. Adsorption in mono-component systems

Fig. 1a and b illustrate the pH effect on CIP and ACE removal. Both pharmaceuticals demonstrated similar removal behaviors, with CIP exhibiting 75–99% removal and ACE showing 91–99% removal, achieving maximum efficiency at natural pH. Since the CH–KOH material exhibits a pH_{PZC} of 7.36 (see Fig. S4), the activated carbon surface remains positively charged at the working pH conditions of 5.93 for CIP and 4.88 for ACE. This surface charge characteristic is crucial for understanding the adsorption mechanism. The adsorption mechanism for CIP arises from its amphoteric properties, characterized by distinct pK_a values. At pH = 5.93, the CH–KOH surface exhibits a net positive charge. At this pH, CIP exists in a balanced state, with 50% in zwitterionic form and 50% in cationic form, facilitating adsorption with its negative charge in zwitterionic form. A similar CIP removal percentage was observed for pH values at 2 and 4 due to the occurrence of electrostatic interactions between the positively charged surface and the CIP zwitterionic form under these conditions, as previously explained. At higher pH values (8 and 10), CIP removal percentages decreased. As the pH levels increase, the adsorbent surface becomes negatively charged, and CIP molecules mainly exist in their anionic form. This results in electrostatic repulsion between the adsorbent surface and the CIP molecules, reducing adsorption efficiency. However, although the removal efficiency is reduced by approximately 20%, this observation highlights the contribution of other adsorption mechanisms beyond electrostatic attraction. The presence of different functional groups on both the activated carbon surface and the contaminant molecules enables the occurrence of other interactions such as formation of hydrogen bonds and π–π interactions under working conditions.

On the other hand, ACE (pK_a 9.5) demonstrates limited electrostatic interactions at pH values below 10, because it is in its neutral form. The consistent removal efficiency across various pH conditions can be attributed to multiple adsorption

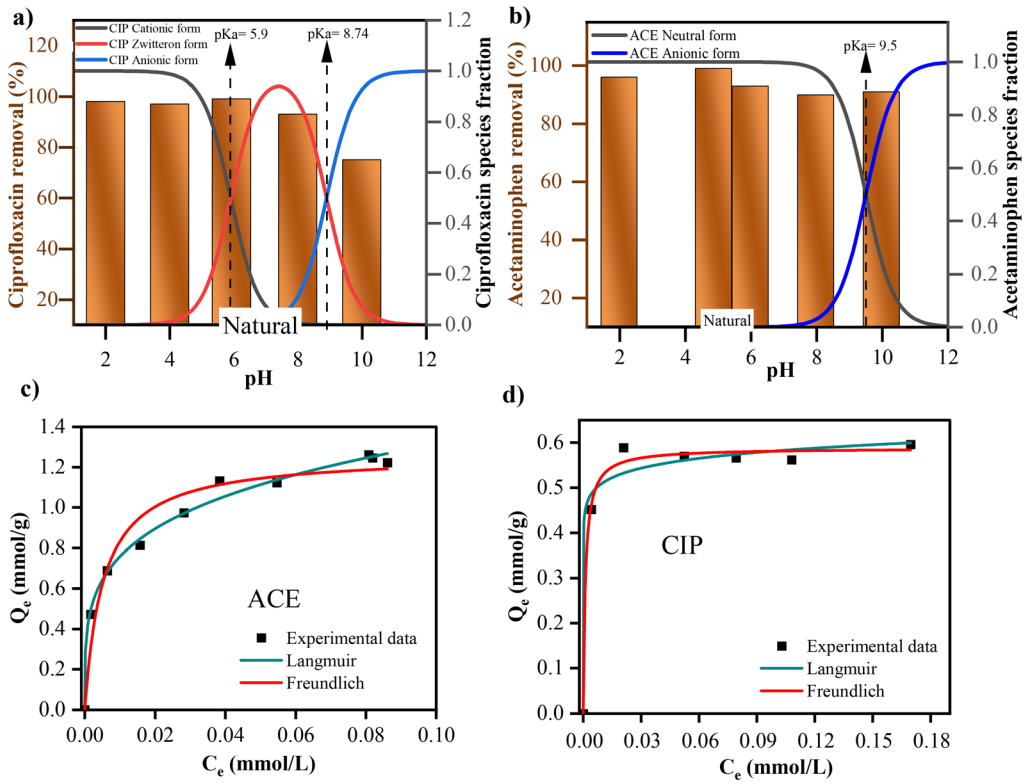

Fig. 1 Adsorption isotherms for a) ACE, and b) CIP, on CH–KOH, adjusted to Freundlich and Langmuir models. Adsorbent dose 0.125 g L^{-1}, initial concentrations of CIP and ACE solutions from 0.06 to 0.24 mmol L^{-1}, optimal contact time: 3 h, controlled pH: 6. Effect of solution pH on the removal of a) CIP and b) ACE using CH–KOH and speciation curves of both contaminants. Conditions: an adsorbent dose of 2.5 g L^{-1}, initial solution concentration of 0.12 mmol ACE per L and 0.26 mmol CIP per L, and 180 min. Adsorption isotherms for c) ACE, and d) CIP, on CH–KOH, adjusted to Freundlich and Langmuir models. Adsorbent dose 0.125 g L^{-1}, initial concentrations of CIP and ACE solutions from 0.06 to 0.24 mmol L^{-1}, optimal contact time: 3 h, controlled pH: 6.

mechanisms not pH-dependent, including pore-filling processes and molecular interactions between the aromatic rings and the carbon structure of this pharmaceutical compound. Therefore, all subsequent experiments were conducted at pH = 6 ensuring optimal adsorption performance and balancing electrostatic and non-electrostatic interactions.

The analysis of the adsorption isotherms for the removal of ACE and CIP using the CH–KOH material reveals important information about the adsorption process. The experimental data were analyzed using the Langmuir and Freundlich models (see Fig. 1c and d). As shown in Table 1, the determination coefficients (R^2_{Adj}) were 0.991 for ACE and 0.979 for CIP, indicating an adequate agreement with the Freundlich model. This suggests that the adsorption process occurs mainly on a heterogeneous surface with multiple adsorption sites of different energy levels. The suitability of the Freundlich model highlights the complex nature of the adsorption mechanism, which likely involves interactions such as multilayer adsorption or surface heterogeneity, consistent with the physicochemical properties of the adsorbent material. These results are related to previous studies where similar behaviors have been reported for adsorption processes on heterogeneous surfaces.[62]

The maximum adsorption capacity, according to the Langmuir model, Q_{max} was significantly higher for ACE (1.26 mmol g^{-1}) compared to CIP (0.58 mmol g^{-1}). The selectivity ratio, S = ($Q_{max,ACE}/Q_{max,CIP}$), derived from the individual adsorption isotherms, indicates that CH–KOH has an ACE adsorption capacity 2.2 times greater than CIP. This suggests that CH–KOH exhibits a higher affinity for ACE molecules in a mono-component system. This behavior can be explained by the different molecular characteristics of the two contaminants and their interaction with the material surface. The CIP adsorption process is highly favored by the occurrence of different chemical interactions. In contrast, the ACE adsorption process is governed by physical adsorption related to a high surface area of CH–KOH material and, to a lesser extent, to the occurrence of chemical interactions between ACE molecules and the carbonaceous material, because of the neutral form of ACE to the evaluated conditions. The values of the n_F parameter of the Freundlich model, which were 0.24 and 0.06 for ACE and CIP, respectively, are less than 1, indicating that adsorption is favorable for both compounds. The lower n_F value for CIP suggests greater heterogeneity in the adsorption process of this compound, which could be related to different interaction mechanisms between the CIP molecule and the adsorbent surface.[63–65]

In comparison with literature-reported adsorbents derived from agricultural wastes (see Table S7), CH–KOH shows competitive adsorption capacities.

For example, KOH-activated coconut husk–kaolinite biochar prepared *via* a microwave technique has been reported to reach a q_m of 0.69 mmol g^{-1} (229 mg g^{-1}) for CIP in batch mode.[65] Activated carbon derived from waste biomass such as peony seed shells, with an ultra-high specific surface area (2980.96 m^2 g^{-1}), achieved CIP removal of 2.36 mmol g^{-1} (Q_{max} = 782.3 mg g^{-1}) in simplified aqueous matrices.[66] Biochar from potato stems and leaves, prepared by pyrolysis at 500 °C and activated with KOH (38.75 m^2 g^{-1}), exhibited a q_m of 0.07 mmol g^{-1} (23.36 mg g^{-1}). In these cases, hydrophobic interactions, hydrogen bonding, electrostatic attraction, and π–π interactions were identified as the main adsorption mechanisms for CIP uptake.[67] In the present study, CH-KOH achieved q_m values of 0.58 mmol g^{-1} for CIP and 1.26 mmol g^{-1} for ACE, maintaining high performance even under multicomponent and continuous-flow conditions.

3.2. Adsorption in multicomponent systems

Bibliometric mapping (Fig. S1, Table S1) reveals that, although CIP and ACE are widely studied, they are rarely addressed in conjunction with fixed-bed adsorption systems. This gap highlights the limited translation of pharmaceutical removal studies from batch-scale tests to realistic continuous-flow configurations, reinforcing the novelty of the present work.

The LME and MLMη_i models were applied to analyze the multicomponent adsorption data and demonstrated satisfactory agreement with the experimental findings. The LME and MLMη_i models exhibited deviation percentages (DESV) of 25.3% and 25.8%, respectively.

Although the LME model showed slightly lower deviation, it is not considered optimal because all of its parameters are determined by fitting competitive adsorption equilibrium data without incorporating individual Langmuir isotherm parameters. In contrast, the MLMη_i model considers the parameters of each isotherm and includes an interaction factor specific to each species. Despite the moderate fitting deviation, MLMη_i provided a more realistic representation of the system compared to traditional isotherm models, supporting its relevance as a first-step predictive tool for complex adsorption processes on heterogeneous surfaces.

The interaction factor values were η_{ACE} = 0.7 and η_{CIP} = 4.9, suggesting that the material's surface has a significantly

Table 1 Parameters of the adsorption isotherm models for CIP and ACE on CH-KOH material

	Langmuir			Freundlich		
	Q_{max} (mmol g^{-1})	K_L (L g^{-1})	R^2_{Adj}	K_F (mmolg^{-1} (L mg^{-1})$^{-1/n}$)	n_F	R^2_{Adj}
CH–KOH–ACE	1.26 ± 0.06	194 ± 50	0.951	2.3 ± 0.1	0.24 ± 0.01	0.991
CH–KOH–CIP	0.58 ± 0.01	863 ± 186	0.992	0.66 ± 0.04	0.06 ± 0.02	0.979

higher affinity for ACE than CIP in multicomponent systems. Specifically, η_{CIP} is seven times larger than η_{ACE}, indicating a stronger competitive effect on CIP adsorption than on ACE adsorption. Moreover, the models of the multicomponent Freundlich isotherm were used to analyze binary adsorption equilibrium data. However, they exhibited deviations greater than 50% and were therefore not considered.

Fig. 2a and b show the MLMη_i model predictions, along with the binary adsorption equilibrium data for CIP and ACE on CH–KOH. Fig. 2a shows the adsorption response surface for ACE adsorption and reveals that CIP presence affected ACE adsorption at low CIP concentrations within the evaluated range (0.04–0.16 mmol L^{-1}). The inhibitory effect was most significant at ACE concentration of 0.007 mmol L^{-1}, where adsorption capacity decreased by 44% compared to the individual system. At higher ACE concentrations (0.11 mmol L^{-1}), however the reduction in adsorption capacity was less pronounced, decreasing by 25.4% relative to the ACE adsorption capacity in the individual system. For CIP adsorption (Fig. 2b), a noticeable effect of ACE presence was observed at lower ACE concentrations (0–0.06 mmol L^{-1}). At these concentrations, the adsorption capacity of CIP decreased by 56% at 0.05 mmol L^{-1} ACE and 33% at 0.06 mmol L^{-1} ACE, respectively compared to the individual system. Additionally, a reduction of nearly 30% was observed at ACE concentrations of 0.07 and 0.15 mmol L^{-1}. These results demonstrate an antagonistic effect and competition between the two pharmaceutical compounds for adsorption sites on CH–KOH, particularly at lower concentrations in the multicomponent system. Additionally, the competitive effects depend on the equilibrium concentration. Fig. 2c shows the total adsorbed mass in the multicomponent system ($qT = q_{ACE} + q_{CIP}$) confirming that both pharmaceuticals compete for the same adsorption sites. This is supported by the fact that qT remains around 1.25 mmol g^{-1} across the entire evaluated concentration range, a value like the Q_{max} found for ACE in the mono-component system.

The competitive adsorption behavior observed in this study aligns with the findings reported by Pauletto, *et al.*[68] regarding acetaminophen–nimesulide binary systems. The presence of the competing pharmaceutical compound significantly impacted ACE adsorption. The authors reported a 28% reduction in ACE adsorption capacity when co-adsorbed with nimesulide. They are attributed to a displacement phenomenon, whereby ACE molecules were released from active sites due to nimesulide's higher affinity for the adsorbent. However, our system exhibited a more concentration-dependent competitive effect, with the strongest inhibition observed at low ACE concentrations. These findings suggest that ACE's adsorption is susceptible to competitive effects, regardless of the competing pharmaceutical compound.

3.3. Adsorption using complex matrices and adsorbent re-use

The performance of the CH–KOH material in adsorbing ACE and CIP from synthetic hospital wastewater and urine was comprehensively evaluated, and the results presented in Fig. 3a. These results demonstrate exceptional performance of CH–KOH in these complex matrices, achieving remarkable removal percentages (84–97%) for both pharmaceuticals. These findings underscore the significant potential of the material for enhancing the removal of pharmaceutical contaminants in wastewater treatment systems. In the case of multicomponent adsorption in complex matrices (Fig. 3b), the performance of CH–KOH exhibited a noticeable decrease in removal efficiency compared to mono-component systems (Fig. 3a), confirming the presence of more pronounced competitive effects under real-world conditions. In synthetic wastewater, CIP and ACE removals ranged from 68% to 100%, whereas in urine, more substantial reductions were observed, with minimum values of 33% for CIP and 60% for ACE depending on the initial molar ratio (mmol L^{-1}) of each pharmaceutical. This behavior can be attributed to simultaneous competition for active adsorption sites, as well as interference from salts, organic compounds, and other species present in the matrices, which modify surface interactions and partially favor one contaminant over the other. Notably, the sharpest decrease was observed for CIP in urine (down to 33%), indicating a higher susceptibility to

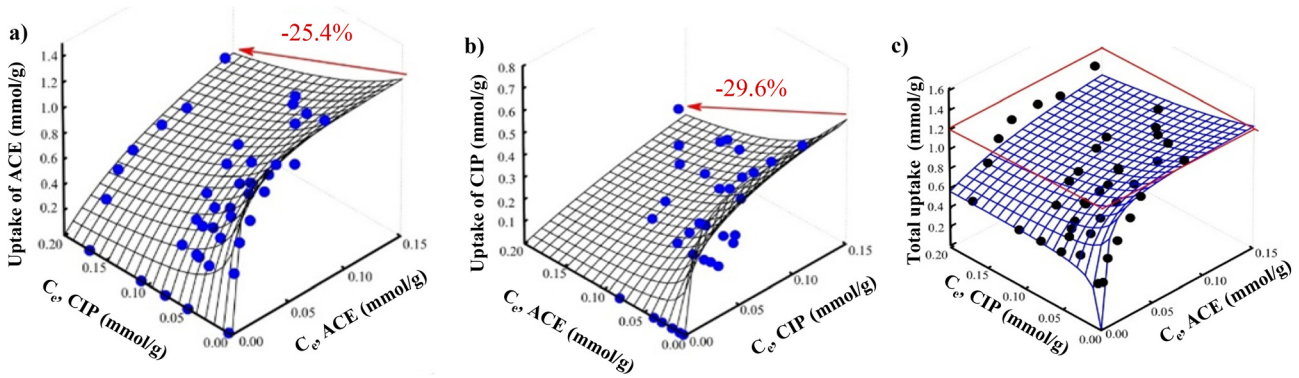

Fig. 2 The adsorption uptakes of both contaminants in the multicomponent systems. a) ACE, b) CIP and c) total uptake in the multicomponent system, $qT = q_{ACE} + q_{CIP}$ (conditions: mass of adsorbent: 0.0125 g, volume of solution: 100 mL, pH = 6, initial concentration of ACE and CIP: 0.06, 0.09, 0.12, 0.15, 0.18, 0.24 mmol L^{-1}, and time 3 h).

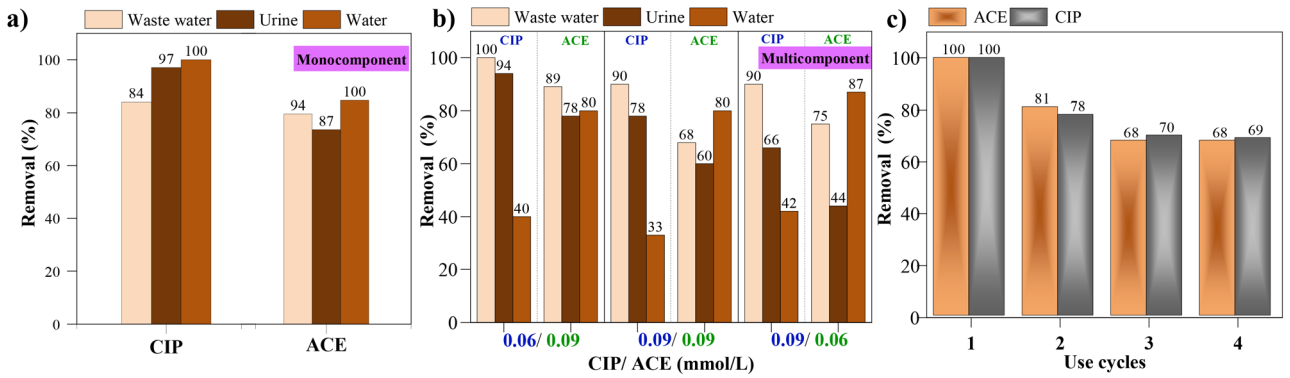

Fig. 3 a) CIP and ACE adsorption in nanocomponent system, showing removal percentages in complex urine and wastewater matrices using CH–KOH; (b) multicomponent adsorption of CIP and ACE (CIP/ACE = 0.06/0.09, 0.09/0.09 and 0.09/0.06 mmol L^{-1}) in complex urine and wastewater matrices; c) reuse cycles of CH–KOH in the adsorption process.

ionic and organic interference, while ACE maintained comparatively higher removal under the same conditions, consistent with its greater affinity observed in equilibrium multicomponent studies. These results confirm that although CH–KOH retains a relevant adsorption capacity in real and complex systems, the magnitude of competitive and matrix effects depends both on the chemical nature of the contaminants and on the solution characteristics.

Fig. 3c shows the adsorbent's performance over multiple adsorption–desorption cycles, a critical factor in assessing the material's practical viability. Reusability is essential for both sustainability and cost-effectiveness. After the first cycle, the material maintained high effectiveness, with only a 20% reduction in removal efficiency. The adsorption capacities decreased from 1.26 to 0.85 mmol g^{-1} for ACE and from 0.58 to 0.40 mmol g^{-1} for CIP, corresponding to approximately 70% removal in both cases. From the third to the fourth cycle, no further decrease in removal capacity was observed for CH–KOH, indicating stable performance after initial use.

This moderate reduction could be attributed to partial active site saturation. The minimal decline suggests that most active sites remain available and functional for subsequent adsorption cycles. The ability of the adsorbent to maintain stable performance across multiple usage cycles demonstrates CH–KOH remarkable chemical and structural stability. This behavior can be ascribed to the unique characteristics of the CH precursor and the chemical activation process using KOH, which generated a material with a robust porous structure and high density of accessible active sites. Furthermore, resistance of the material to structural degradation or porosity collapse indicates that the activation process produced a substrate with exceptional mechanical and chemical resilience. CH–KOH's consistent removal capacity throughout multiple cycles suggests its potential applicability in continuous treatment systems or batch treatment applications, where long-term stability is essential. This stability also minimizes the need for frequent regeneration, consequently reducing operational costs and secondary waste generation. CH–KOH is an attractive candidate for large-scale implementation in advanced water treatment technologies.

3.4. Adsorption in continuous systems

Continuous adsorption experiments were conducted in fixed-bed columns to evaluate the effectiveness of CH–KOH in removing CIP and ACE. These experiments assessed the effects of flow rate, bed height, and initial concentration. The resulting breakthrough curves are presented in Fig. 4. Table 2 summarizes the corresponding curve parameters. The curves were interpreted by the Thomas and Clark models and the resulting parameters obtained are shown in Table S6. The Thomas model accurately interprets the experimental data for the two pharmaceutical compounds, yielding high determination coefficients. Fig. 4a shows that that ACE exhibits symmetrical breakthrough curve behavior at different flow rates, indicating rapid adsorption kinetics and efficient contaminant removal. The mass transfer zone (MTZ) calculations supported this observation, because large MTZ typically indicates slow adsorption kinetics. The calculated MTZ for ACE occupied approximately half of the bed height, suggesting efficient mass transfer. The saturation capacity (q_s) under continuous flow closely matched the equilibrium capacity obtained in batch experiments, confirming the material's effectiveness under dynamic conditions. CIP breakthrough curves (Fig. 4b) also displayed symmetrical behavior but with more extended sigmoidal profiles. The greater separation between the breakthrough and saturation points is reflected in significantly larger MTZ values compared to those of ACE, which indicates slower adsorption kinetics for CIP. At higher flow rates (2 and 3 mL min^{-1}), breakthroughs occurred almost simultaneously, suggesting insufficient residence time for optimal CIP removal The influence of bed height on adsorption performance was investigated by conducting experiments with heights ranging from 1 to 3 cm for both ACE and CIP. As shown in Fig. 4c and d, increasing the bed height delayed both breakthrough and saturation times. This is consistent with the increased availability of active sites provided by a larger

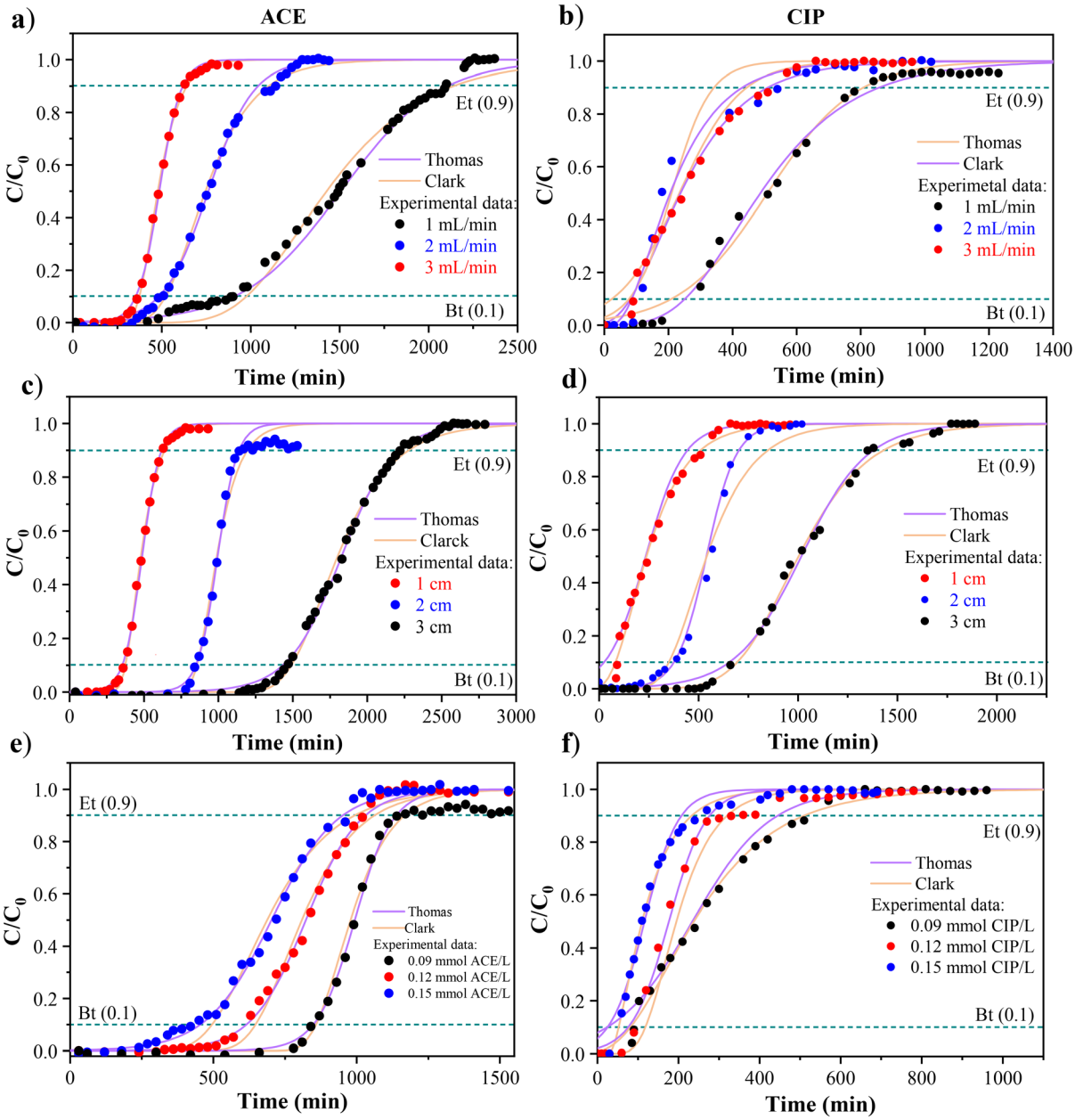

Fig. 4 Adsorption in continuous systems a) and b) effect of flow on breakthrough curves (conditions: a) 1 cm, 0.09 mmol ACE per L; b) 1 cm, 0.09 mmol CIP per L). c) and d) Effect of bed height on breakthrough curves under the following (conditions: c) 3 mL min^{-1}, 0.09 mmol ACE per L; d) 2 mL min^{-1}, 0.09 mmol CIP per L). e) and f) Effect of feed concentration on breakthrough curves (conditions: e) 2 cm, 3 mL min^{-1}; f) 1 cm, 2 mL min^{-1}). E_t: exhaustion time = 0.9, B_t: breakthrough time = 0.1.

adsorbent mass. Breakthrough time exhibited a linear relationship with bed height for both pharmaceuticals, aligning with previous findings in the literature.[69] When the bed height increased from 1 to 2 cm, the MTZ remained relatively constant for both compounds, as evidenced by a rightward shift in the breakthrough curves. However, increasing the bed height to 3 cm resulted in curve flattening, indicating an extended mass transfer zone. This phenomenon can be attributed to the increased contact time at greater bed heights, which enables more efficient utilization of the adsorbent's active sites. This effect was particularly evident in the saturation capacities observed at 3 cm bed height, where both pharmaceuticals achieved adsorption capacities comparable to those obtained from equilibrium isotherms. This indicates optimal material utilization. The effect of the initial feed concentration was investigated by varying concentrations from 0.09 to 0.15 mmol L^{-1} for ACE and from 0.09 to 0.15 mmol L^{-1} for CIP (see Fig. 4e and f). For ACE, increasing the initial concentration led to accelerated breakthrough times. This was due to a fixed number of active sites processing a higher contaminant load, resulting in faster adsorbent saturation.

Table 2 Characteristic parameters of breakthrough curves in flow optimization in adsorption packed column assembly

Column characteristics								
Flow (mL min^{-1})		t_b (min)	t_s (min)	MTZ (cm)	q_e (mmol g^{-1})	q_s (mmol g^{-1})	Adsorbent mass (g)	U_r (g L^{-1})
ACE								
a)	1	904.71	2095.17	0.57	0.71	1.17	0.12	0.13
	2	499.75	1140.06	0.56	0.78	1.20	0.12	0.12
	3	365.04	625.60	0.42	0.90	1.23	0.12	0.11
CIP								
b)	1	287.20	820.25	0.65	0.23	0.43	0.12	0.42
	2	91.17	532.92	0.83	0.15	0.44	0.12	0.66
	3	110.65	544.70	0.80	0.28	0.61	0.12	0.36
Bed (cm)		t_b (min)	t_s (min)	MTZ (cm)	q_e (mmol g^{-1})	q_s (mmol g^{-1})	Adsorbent mass (g)	U_r (g L^{-1})
ACE								
c)	1	365.04	625.60	0.42	0.90	1.23	0.12	0.33
	2	845.50	1227.40	0.62	1.04	1.26	0.24	0.14
	3	1462.64	2222.17	1.03	1.16	1.46	0.36	0.08
CIP								
d)	1	91.17	532.92	0.83	0.15	0.44	0.12	1.32
	2	370.06	708.36	0.96	0.27	0.42	0.24	0.32
	3	664.79	1354.50	1.53	0.37	0.58	0.36	0.18
Concentrations (mmol L^{-1})		t_b (min)	t_s (min)	MTZ (cm)	q_e (mmol g^{-1})	q_s (mmol g^{-1})	Adsorbent mass (g)	U_r (g L^{-1})
ACE								
e)	0.09	845.50	1227.40	0.62	1.04	1.26	0.24	0.09
	0.12	605.03	1024.06	0.82	0.89	1.23	0.24	0.13
	0.15	429.17	968.37	1.11	0.80	1.37	0.24	0.19
CIP								
f)	0.09	91.17	532.92	0.83	0.15	0.44	0.12	0.65
	0.12	93.86	338.25	0.72	0.19	0.41	0.12	0.63
	0.15	49.64	253.78	0.80	0.13	0.36	0.12	1.19

CIP exhibited similar breakthrough acceleration with increased concentration. However, the breakthrough curves displayed reduced amplitude and decreased flattening at higher concentrations (see Fig. 4f). This phenomenon is consistent with previous literature and can be attributed to enhanced mass transfer resulting from steeper concentration gradients at higher feed concentrations.[70]

Table 2 includes the usage ratio (U_r), which represents the volume of solution treated per gram of adsorbent up to the breakthrough point. For ACE, U_r values ranged from 0.08 g L^{-1} to 0.33 g L^{-1}, whereas for CIP, U_r values ranged from 0.18 g L^{-1} to 1.32 g L^{-1}. These results clearly indicate that, under continuous operation, the removal of CIP is more efficient than that of ACE.

3.5. Proposed adsorption mechanisms

Characterization before and after adsorption enables identification of changes in the adsorbent material and confirmation of possible adsorption mechanisms. SEM–EDS elemental mapping and SEM micrographs (see Fig. 5) showed that CH–KOH shows a well-developed porous structure, which is characteristic of KOH activation.[71] No significant morphological changes were observed after adsorption of ACE and CIP (see Fig. 5b). Elemental mapping revealed the presence of C, O, N, F and Si in CH–KOH. SEM–EDS semi-quantitative analysis confirmed the presence of minor elements like Mg and Ca and detected F and N after adsorption. Notably, N appeared only in the dual-contaminant system.

Spectroscopic characterization techniques were employed to confirm the interactions between CH–KOH and the contaminants. Fig. 6 shows: a) the FTIR spectrum in the range of 3950–3000 cm^{-1}, b) the FTIR spectra deconvolution in the range of 1700–1300 cm^{-1}, c) the FTIR spectra deconvolution in the range of 1300–450 cm^{-1}, d) the second derivative of the FTIR spectra, which was used to identify the main functional group bands during the deconvolution process, and e) XRD patterns, which confirm the presence of elements identified by SEM–EDS. Additionally, difference spectra before and after adsorption, presented in Fig. S5, were employed to identify new band positions and the reduction of specific peaks. The FTIR spectra reveal characteristic O–H group signals at 3384 and 3206 cm^{-1}, indicating the presence of these functional groups before and after adsorption. In the 1700–1300 cm^{-1} region, CH–KOH exhibits signals at 1619 cm^{-1}, 1580 cm^{-1}, 1548 cm^{-1}, and 1507 cm^{-1}, which can be assigned to aromatic (Ar) C=C, and reflect the presence of diverse aromatic structures. The band at 1471 cm^{-1} can be assigned to υC–O and –CH_2, which aligns with the structural complexity typically found in activated carbon materials.[71] Signals in the 1300–450 cm^{-1} range confirm oxygen-containing functional groups, with peaks at 1214 cm^{-1} (Ar–C–O), 1150 cm^{-1} (C–O, ester), 1074 cm^{-1} (C–OH), 1020 cm^{-1}, and 957 cm^{-1} (C–O).[54] The CH–KOH–ACE sample shows new bands at 1576 cm^{-1}, which correspond to C=C–N–H bending (amide); at 1540 cm^{-1} for C–N–C=O stretching (amide); at 1500 cm^{-1} for aromatic C=C, 1481 cm^{-1} assigned to –CH_3 antisymmetric bending; at 1465 cm^{-1} for O–H in-plane bending; at 802 cm^{-1} for C–H aromatic out-of-plane bending, and 769 cm^{-1} for C=C.

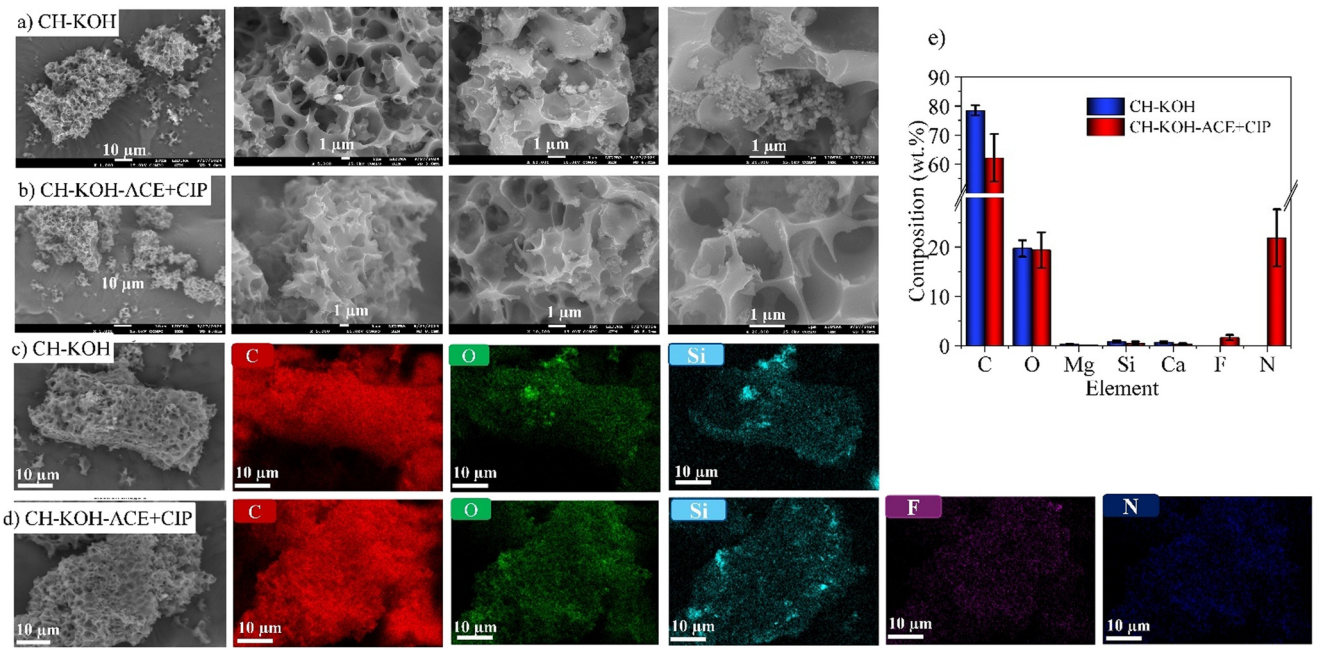

Fig. 5 a) SEM micrographs of KOH-activated adsorbents (CH–KOH), b) CH–KOH after acetaminophen and ciprofloxacin adsorption (CH–KOH–ACE + CIP), c) SEM–EDS elemental mapping of CH–KOH, d) SEM–EDS elemental mapping of CH–KOH after acetaminophen and ciprofloxacin adsorption (CH–KOH–ACE + CIP), and e) weight percentage of detected elements.

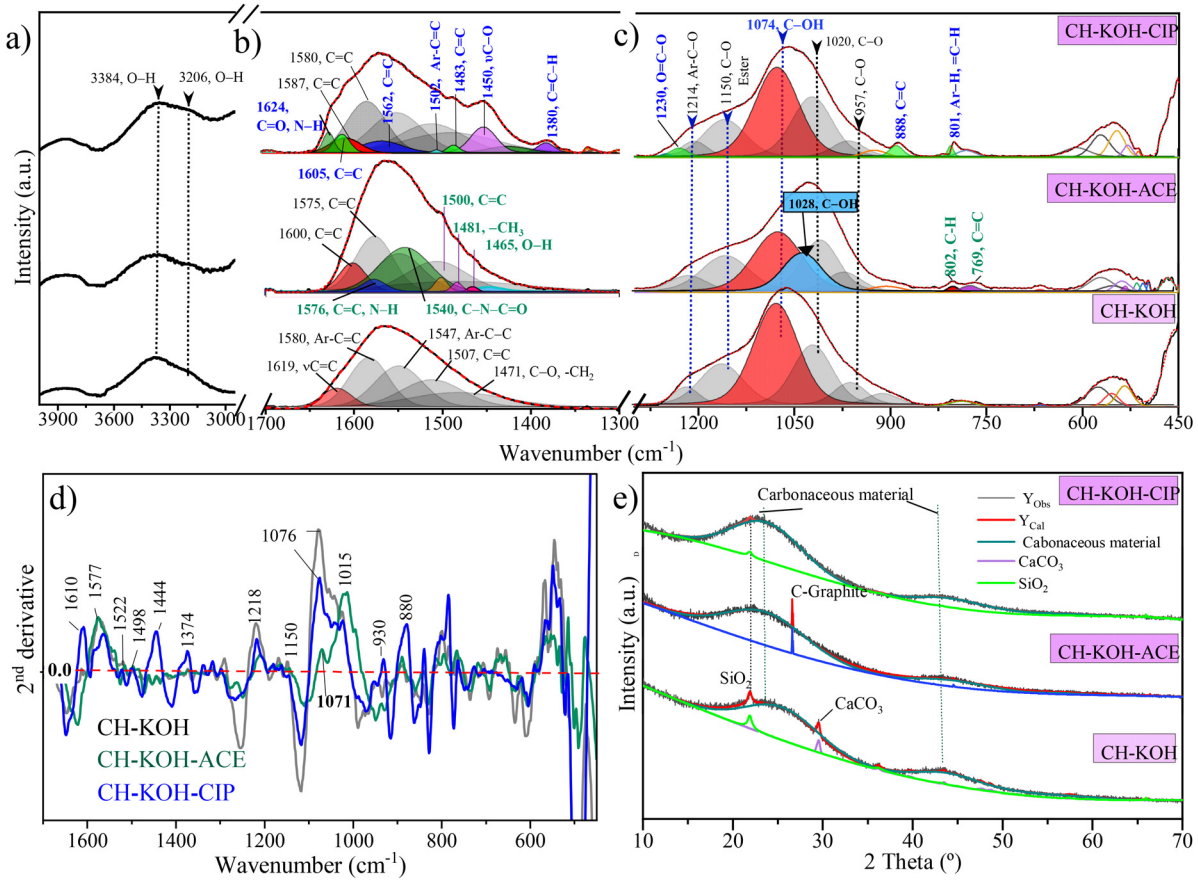

Fig. 6 FTIR and XRD characterization of CH–KOH before and after the adsorption of ciprofloxacin (CH–KOH–CIP) and acetaminophen (CH–KOH–ACE), a) FTIR spectrum in the range of 3950–3000 cm^{-1}, b) FTIR spectra deconvolution in the range of 1700–1300 cm^{-1}, c) FTIR spectra deconvolution in the range of 1300–450 cm^{-1}, d) second derivative of FTIR spectra used to identify the main functional group bands during the deconvolution process, and e) XRD patterns.

Additionally, the C–OH band at 1074 cm^{-1} in the CH–KOH sample weakens, and a new band appears at 1028 cm^{-1}. These changes indicate strong interactions between the phenolic groups of CH–KOH and ACE, consistent with the structural behavior of ACE at higher pH levels (see Fig. 1b). In these conditions, the phenolic–OH group contributes to the FTIR band shift from 1074 to 1028 cm^{-1}.[72] After CIP adsorption, however, the CH–KOH–CIP spectrum in the 1700–1300 cm^{-1} range shows new signals at 1607 cm^{-1}, which correspond to C═O bond vibrations or quinolone N–H bending vibration. In the 1300–1500 cm^{-1} range, new peaks appear at 1562 cm^{-1}, 1502 cm^{-1}, and 1483 cm^{-1} for aromatic C═C, along with bands at 1450 cm^{-1} for *νC*–O and 1380 cm^{-1} for C–H. Additionally, signals are observed at 1230 cm^{-1}, which are assigned to C–O in O═C–O, and at 888 cm^{-1} and 801 cm^{-1} C═C and C–H respectively for the aromatic structure.[73] These bands confirm the presence of CIP.

The XRD patterns (Fig. 6e, and Table S8), CH–KOH show two broad Bragg peaks at 22.0° and 43.7°, which correspond to the (002) and (100) planes, respectively. These peaks are characteristic of the hexagonal graphite structure. These broad peaks are typical of amorphous carbon materials.[74] Additionally, two low-intensity peaks were identified: one at 2θ = 21.6°, which was assigned to the (111) plane of SiO_2 (ICSD 162659) with a 1.1 wt% according to the Rietveld refinement, and another at 2θ = 29.6°, which was associated with the (11–2) plane of $CaCO_3$ (ICSD collection code: 150) with a 0.7 wt%. After the adsorption of ACE and CIP, the peak corresponding to $CaCO_3$ was no longer observed. Nevertheless, the material continues to exhibit the characteristic peaks for the (002) and (100) planes of the carbonaceous structure of activated carbon, No $CaCO_3$ was present, and only 0.7 wt% of SiO_2 was detected in CH–KOH–CIP.

Fig. 7 and Table S9 present the XPS analysis of (a) C1s, (b) O1s, (c) N1s, and (d) F1s before and after the adsorption of ACE and CIP, revealing significant changes in the signals corresponding to the main elements (C, O, N, and F). In the CH–KOH sample, the following C1s contributions were identified: C═C (60.3 at%), C–C (15.0 at%), C–OH (14.2 at%), C═O (6.4 at%), and O═C–O (4.1 at%). After adsorption, these values changed to C═C (48.6 at%), C–C (21.2 at%), C–OH (19.5 at%), C═O (7.2 at%), and O═C–O (3.4 at%), indicating an increase in C–OH and C═O groups.[74]

For O1s, prior to adsorption, peaks were observed at 531.8 eV for aromatic O═C (27.7 at%), 533.1 eV for

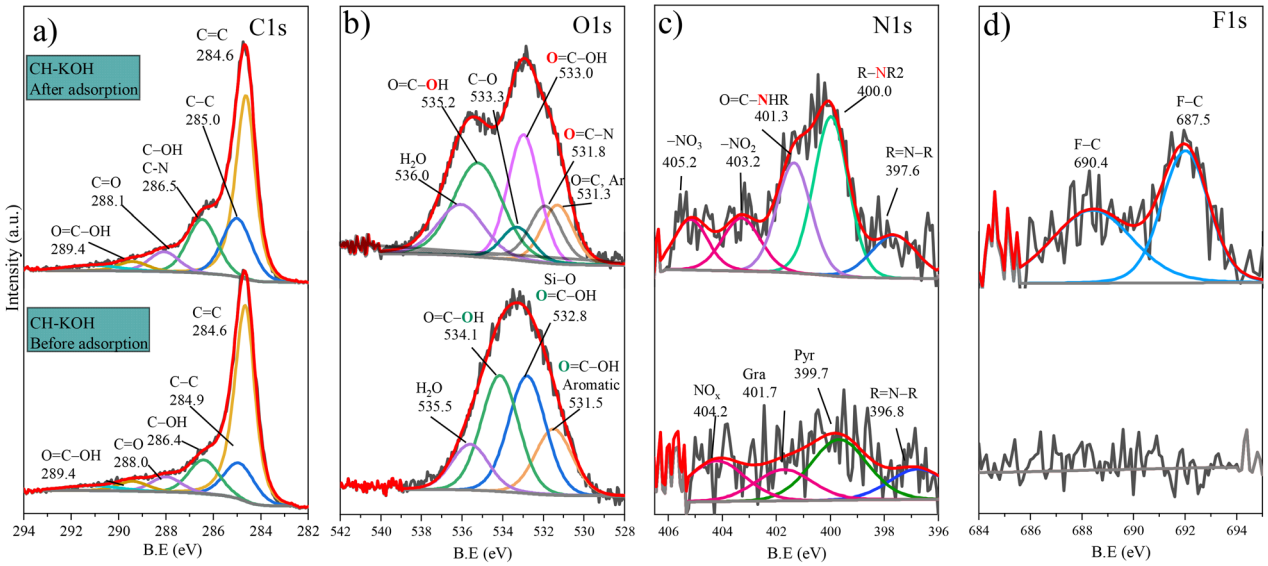

Fig. 7 XPS spectra of the adsorbent material before adsorption (bottom) and after adsorption (top) of a solution containing both contaminants, acetaminophen (ACE) and ciprofloxacin (CIP): a) C1s, b) O1s, c) N1s, and d) F1s.

O═C–OH (30.7 at%), 534.2 eV for O–H in O═C–OH (32.4 at%), and 535.5 eV for adsorbed water (9.2 at%). After adsorption, a shift in the O═C–OH signal was observed around 535 eV (39.1 at%), along with the appearance of a new peak at 533.30 eV assigned to C–O (8.9 at%), both representing oxygen in O–C and O═C within the O═C–OH (11.6 at%) group. Additionally, a new signal at 531.8 eV was detected and attributed to oxygen in the O═C–N (14.8 at%) group of ACE.

Initially, the N1s spectrum of CH–KOH displayed peaks at 399.7 eV (37.4 at%) for pyrrolic nitrogen (Pyr), 401.7 eV (19.0 at%) for graphitic nitrogen (Gra), and 404.2 eV (25.0 at%) for

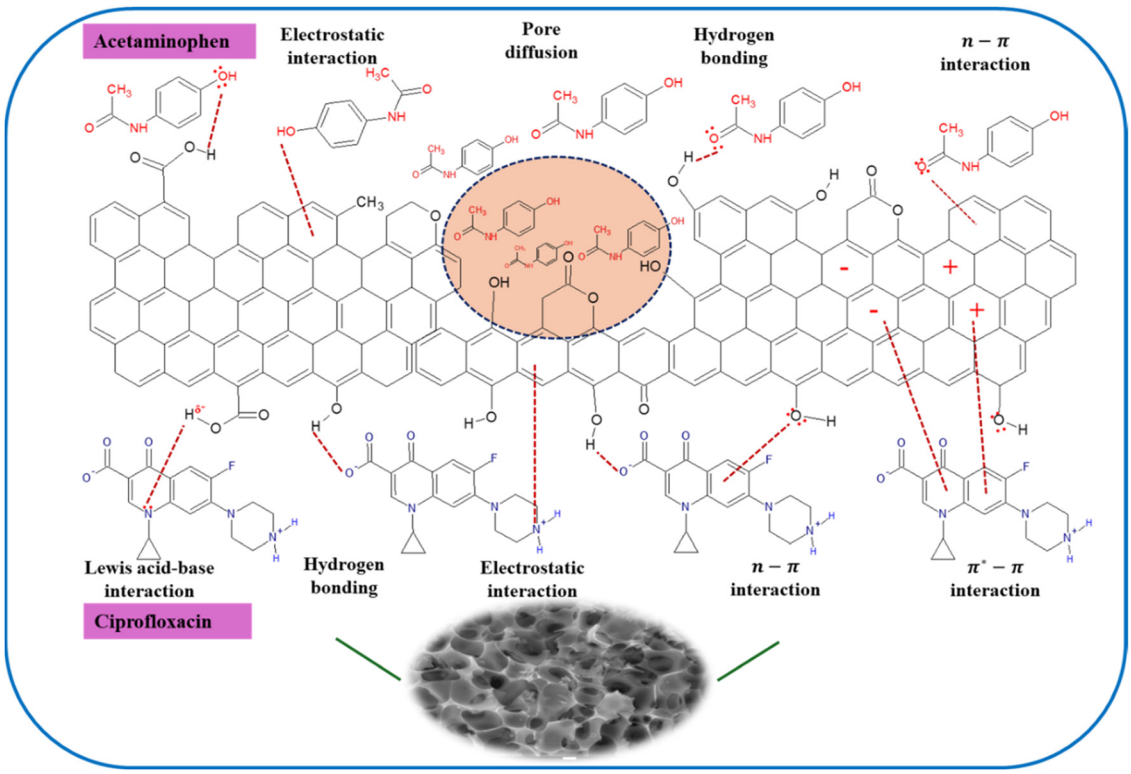

Fig. 8 Various mechanisms of CH–KOH and interaction with acetaminophen (ACE) and ciprofloxacin (CIP).

NO_x species. After adsorption, new bands appeared at 400.1 eV (35.2 at.%), attributed to the C–NR_2 group, and at 401.3 eV (25.4 at%), corresponding to the O═C–NHR group for ACE and CIP, respectively.

Finally, the F1s spectra exhibited peaks at 687.5 eV (51.3 at%) and 690.4 eV (48.7 at%). Although small, the signal at 690.4 eV suggests an interaction between fluorine and the activated carbon surface.[75]

Fig. 8 summarizes the main mechanisms identified in the adsorption of ACE and CIP onto CH–KOH. Based on information obtained from the adsorption experiments and material characterization, the adsorption mechanism is primarily governed by physisorption, involving non-covalent interactions such π^+–π interactions, hydrophobic interactions, hydrogen bonding, and van der Waals forces.

For ACE, the molecules remain nearly neutral across the evaluated pH values. Non-electrostatic interactions may include hydrogen bonding, π–π interactions, n–π electron donor–acceptor interactions, and hydrophobic–hydrophobic interactions. CH–KOH has various polar surface functionalities, such as –OH and –COOH groups, that can interact with the –OH and –NH moieties in ACE molecules through hydrogen bonding. This was evidenced by the differences observed in the FTIR spectra. ACE adsorption on the CH–KOH surface can also occur *via* π–π interactions between the π electrons of the fused conjugated aromatic moieties in CH–KOH (donor) and the π electrons in the benzene ring of ACE (acceptor). ACE adsorption can also occur through n–π electron donor–acceptor interactions between the lone pair of electrons on the oxygen in the surface carbonyl groups of CH–KOH (electron donors) and the benzene ring of ACE (electron acceptor). The significant contribution of the π–π mechanism to ACE sorption is further supported by the adsorption capacity remaining nearly unchanged under varying pH conditions, as shown in Fig. 1, given that π–π interactions are pH-independent. Additionally, pore diffusion is expected to play a substantial role in the uptake of ACE.

Conclusions

This study demonstrated the potential of CH–KOH as a sustainable and efficient adsorbent for the removal of multiple pharmaceutical contaminants under complex and realistic conditions. The valorization of CH biomass significantly enhanced its physicochemical properties, generating a material with a high BET surface area (1145 m^2 g^{-1}), well-developed microporosity, and enriched oxygenated functional groups that boosted adsorption performance. In mono-component systems, CH–KOH reached a Q_{max} of 1.26 mmol g^{-1} for ACE and 0.58 mmol g^{-1} for CIP, with removal efficiencies of 91–99% and 75–99%, respectively. Importantly, CH–KOH maintained excellent performance in complex real-like matrices such as synthetic hospital wastewater and urine, achieving 84–97% removal in mono-component systems and robust adsorption despite competitive and matrix effects, with minimum values of 60% for ACE and 33% for CIP in urine.

The multicomponent adsorption data were described by the MLMη_i model, indicating significantly higher affinity for ACE (η_{ACE} = 0.7) than for CIP (η_{CIP} = 4.9), with a qT of 1.25 mmol g^{-1} like the Q_{max} found for ACE in the mono-component system. Competitive effects were concentration-dependent, with ACE reducing CIP adsorption by up to 44% and CIP reducing ACE adsorption by up to 25%.

The potential for application in real treatment systems is reinforced by the systematic evaluation in multicomponent batch systems and in continuous fixed-bed columns. In columns, CH–KOH reached saturation capacities (q_s) up to 1.46 mmol g^{-1} for ACE and 0.61 mmol g^{-1} for CIP, with mass transfer zones of 0.42–1.53 cm and breakthrough times from 91 to 1463 min depending on flow rate (1–3 mL min^{-1}) and bed height (1–3 cm). The Thomas model successfully described the breakthrough behavior, confirming faster kinetics for ACE.

Physisorption predominates, involving synergistic π–π stacking interactions, hydrogen bonding networks, and hydrophobic association, supported by detailed characterization before and after adsorption (FTIR, XRD, XPS, SEM–EDS), which confirmed the interactions between the adsorbent and contaminants and verified the stability of the material's structure.

Reusability studies showed that CH–KOH maintained ~70% removal capacity after three adsorption–desorption cycles, and no further gradual loss in adsorption capacity beyond the third cycle, demonstrating its long-term stability. The combination of biomass valorization, enhanced adsorption properties from KOH activation, strong performance in complex matrices, detailed mechanistic understanding, and operational stability highlights CH–KOH as a promising adsorbent for large-scale pharmaceutical contaminant removal, fully aligned with sustainable and circular economy strategies.

Author contributions

Valentina Ospina-Montoya: conceptualization, methodology, investigation, data curation, writing – original draft. Samuel Aguirre-Contreras: methodology, formal analysis, writing – original draft. Raúl Ocampo-Pérez: conceptualization, methodology, validation, supervision, writing – review & editing. Erika Padilla-Ortega: formal analysis, data curation, validation, writing – review & editing. Sebastián Pérez: conceptualization, data curation, methodology, investigation, software, formal analysis, writing – original draft. Juan Muñoz-Saldaña: investigation, resources, writing – review & editing. Jazmín Porras: conceptualization, methodology, supervision, project administration, writing – review &

editing, funding acquisition. Nancy Acelas: conceptualization, methodology, validation, resources, writing – review & editing. Angélica Forgionny: conceptualization, methodology, investigation, software, formal analysis, data curation, visualization, writing – review & editing, project administration, funding acquisition.

Conflicts of interest

There are no conflicts to declare.

Dataavailability

Supplementary information: The SI provides detailed methodologies, equations, bibliometric analysis, experimental data, and additional results. It includes adsorption modeling approaches (Langmuir, Freundlich, and multicomponent models), column adsorption experiments, physicochemical characterization of the materials, and comparative analyses with existing literature. Supplementary figures and tables present bibliometric maps, adsorption capacities, FTIR, XRD, and XPS data, as well as the chemical composition of the synthetic matrices, providing extended evidence for the adsorption performance of KOH-activated coffee husk in removing ACE and CIP under multicomponent and continuous-flow conditions. See DOI: **https://doi.org/10.1039/D5EW00499C**.

The authors confirm that the data supporting the findings of this study are available within the article.

Acknowledgements

The authors from the University of Medellín and UniRemington express their gratitude to their respective institutions for the financial support provided for the project 1241 and 4000000425, respectively. Also, the authors thank the Delfín program for the participation of students from different Mexican universities within the framework of the XXVIII Pacific Scientific and Technological Research Summer. We are also grateful for the facilities granted in the use of LIDTRA infrastructure, through the projects: LN295261, LN254119, and LN299082; as well as Liliana's technical assistance. Sebastián Pérez thanks to the Secretaría de Ciencia, Humanidades, Tecnología e Innovación (SECIHTI) for his Ph.D. scholarship with the number 1182859.

References

1 X. Li, X. Shen, W. Jiang, Y. Xi and S. Li, *Ecotoxicol. Environ. Saf.*, 2024, **278**, 116420.
2 J. Beaman, W. Co-chair, D. Eignor and L. Huff, *Aquatic life criteria for contaminants of emerging concern*, 2008.
3 N. Ranjan, P. K. Singh and N. S. Maurya, *Ecotoxicol. Environ. Saf.*, 2022, **247**, 114220.
4 M. Ortúzar, M. Esterhuizen, D. R. Olicón-Hernández, J. González-López and E. Aranda, *Front. Microbiol.*, 2022, **13**, 1–25.
5 S. M. F. Mariano, L. F. Angeles, D. S. Aga, C. L. Villanoy and C. M. B. Jaraula, *Front. Earth Sci.*, 2023, **11**, 1–15.
6 K. Samal, S. Mahapatra and M. Hibzur Ali, *Energy Nexus*, 2022, **6**, 100076.
7 M. Hejna, D. Kapuścińska and A. Aksmann, *Int. J. Environ. Res. Public Health*, 2022, **19**(13), 7717.
8 J. L. Wilkinson, A. B. A. Boxall, D. W. Kolpin, K. M. Y. Leung, R. W. S. Lai, D. Wong, R. Ntchantcho, J. Pizarro, J. Mart, S. Echeverr, J. Garric, A. Chaumot, P. Gibba, I. Kunchulia, S. Seidensticker, G. Lyberatos, J. M. Morales-salda and H. Kang, *Proc. Natl. Acad. Sci. U. S. A.*, 2022, **119**, 1–10.
9 D. Azizi, A. Arif, D. Blair, J. Dionne, Y. Filion, Y. Ouarda, A. G. Pazmino, R. Pulicharla, V. Rilstone, B. Tiwari, L. Vignale, S. K. Brar, P. Champagne, P. Drogui, V. S. Langlois and J. F. Blais, *Environ. Res.*, 2022, **207**, 112196.
10 A. Chakraborty, S. Adhikary, S. Bhattacharya, S. Dutta, S. Chatterjee, D. Banerjee, A. Ganguly and P. Rajak, *ACS Chem. Health Saf.*, 2023, **30**, 362–388.
11 B. Nunes, S. C. Antunes, J. Santos, L. Martins and B. B. Castro, *Ecotoxicol. Environ. Saf.*, 2014, **107**, 178–185.
12 D. R. Lima, A. Hosseini-Bandegharaei, P. S. Thue, E. C. Lima, Y. R. T. de Albuquerque, G. S. dos Reis, C. S. Umpierres, S. L. P. Dias and H. N. Tran, *Colloids Surf., A*, 2019, **583**, 123966.
13 C. Bhagat, M. Kumar, V. K. Tyagi and P. K. Mohapatra, *npj Clean Water*, 2020, **3**, 42.
14 A. M. Botero-Coy, D. Martínez-Pachón, C. Boix, R. J. Rincón, N. Castillo, L. P. Arias-Marín, L. Manrique-Losada, R. Torres-Palma, A. Moncayo-Lasso and F. Hernández, *Sci. Total Environ.*, 2018, **642**, 842–853.
15 M. Gros, M. Petrović, A. Ginebreda and D. Barceló, *Environ. Int.*, 2010, **36**, 15–26.
16 P. Verlicchi, M. Al Aukidy and E. Zambello, *Sci. Total Environ.*, 2012, **429**, 123–155.
17 J. Matesun, L. Petrik, E. Musvoto, W. Ayinde and D. Ikumi, *Ecotoxicol. Environ. Saf.*, 2024, **281**, 116610.
18 V. Ospina-Montoya, V. Cardozo, J. Porras, N. Acelas and A. Forgionny, *H2Open J.*, 2024, **7**, 303–317.
19 S. Ahmadzadeh, A. Asadipour, M. Pournamdari, B. Behnam, H. R. Rahimi and M. Dolatabadi, *Process Saf. Environ. Prot.*, 2017, **109**, 538–547.
20 E. A. Serna-Galvis, J. Silva-Agredo, F. Hernández, A. M. Botero-Coy and R. A. Torres-Palma, *MethodsX*, 2023, **10**, 102128.
21 J. Park, C. Kim, Y. Hong, W. Lee, H. Chung, D. H. Jeong and H. Kim, *Int. J. Environ. Res. Public Health*, 2020, **17**(3), 687.
22 J. Cevallos-Mendoza, C. G. Amorim, J. M. Rodríguez-Díaz and M. Montenegro, *Membranes*, 2022, **12**, 1–23.
23 L. Qalyoubi, A. Al-Othman and S. Al-Asheh, *Environ. Res.*, 2022, **215**, 114182.
24 G. Ren, H. Han, Y. Wang, S. Liu, J. Zhao, X. Meng and Z. Li, *Nanomaterials*, 2021, **11**(7), 1804.
25 M. Patel, R. Kumar, C. U. Pittman and D. Mohan, *Environ. Res.*, 2021, **201**, 111218.
26 O. A. Ajala, S. O. Akinnawo, A. Bamisaye, D. T. Adedipe, M. O. Adesina, O. A. Okon-Akan, T. A. Adebusuyi, A. T.

Ojedokun, K. A. Adegoke and O. S. Bello, *RSC Adv.*, 2023, **13**, 4678–4712.
27 M. El Saied, S. A. Shaban, M. S. Mostafa and A. O. A. El Naga, *Biomass Convers. Biorefin.*, 2024, **14**, 2155–2172.
28 M. Salih, B. Y. Abdulkhair and M. Alotaibi, *Chemistry*, 2023, **5**, 1870–1881.
29 J. G. Carriazo, M. J. Saavedra and M. F. Molina, *Educ. Quim.*, 2010, **21**, 224–229.
30 G. C. C. Ortega, C. C. A. Viloria, B. C. A. Morrinson, M. E. R. Angulo and A. A. M. Zambrano, *Rev. Colombiana Cienc. Anim. - RECIA*, 2017, **9**, 164–170.
31 A. O. Abo El Naga, M. El Saied, S. A. Shaban and F. Y. El Kady, *J. Mol. Liq.*, 2019, **285**, 9–19.
32 S. Rovani, M. T. Censi, S. L. Pedrotti, É. C. Lima, R. Cataluña and A. N. Fernandes, *J. Hazard. Mater.*, 2014, **271**, 311–320.
33 S. Wong, Y. Lim, N. Ngadi, R. Mat, O. Hassan, I. M. Inuwa, N. B. Mohamed and J. H. Low, *Powder Technol.*, 2018, **338**, 878–886.
34 M. R. Cunha, E. C. Lima, N. F. G. M. Cimirro, P. S. Thue, S. L. P. Dias, M. A. Gelesky, G. L. Dotto, G. S. dos Reis and F. A. Pavan, *Environ. Sci. Pollut. Res.*, 2018, **25**, 23315–23327.
35 T. P. de Araújo, H. B. Quesada, R. Bergamasco, D. T. Vareschini and M. A. S. D. de Barros, *Bioresour. Technol.*, 2020, **310**, 123399.
36 A. B. Leite, C. Saucier, E. C. Lima, G. S. dos Reis, C. S. Umpierres, B. L. Mello, M. Shirmardi, S. L. P. Dias and C. H. Sampaio, *Environ. Sci. Pollut. Res.*, 2018, **25**, 7647–7661.
37 A. H. Jawad and A. S. Abdulhameed, *Energy, Ecol. Environ.*, 2020, **5**, 456–469.
38 R. N. Coimbra, V. Calisto, C. I. A. Ferreira, V. I. Esteves and M. Otero, *Arabian J. Chem.*, 2019, **12**, 3611–3620.
39 G. S. dos Reis, M. Guy, M. Mathieu, M. Jebrane, E. C. Lima, M. Thyrel, G. L. Dotto and S. H. Larsson, *Colloids Surf., A*, 2022, **642**, 128626.
40 L. Spessato, K. C. Bedin, A. L. Cazetta, I. P. A. F. Souza, V. A. Duarte, L. H. S. Crespo, M. C. Silva, R. M. Pontes and V. C. Almeida, *J. Hazard. Mater.*, 2019, **371**, 499–505.
41 A. Michelon, J. Bortoluz, C. S. Raota and M. Giovanela, *Environ. Adv.*, 2022, **9**, 100261.
42 A. H. Nordin, A. S. Norfarhana, S. F. M. Noor, S. H. Paiman, M. L. Nordin, S. M. N. Husna, R. A. Ilyas, N. Ngadi, A. A. Bakar, Z. Ahmad, M. S. Azami, W. I. Nawawi and W. Nabgan, *Separations*, 2023, **10**(5), 300.
43 K. Pongsiriyakul, P. Wongsurakul, W. Kiatkittipong, A. Premashthira, K. Kuldilok, V. Najdanovic-Visak, S. Adhikari, P. Cognet, T. Kida and S. Assabumrungrat, *Processes*, 2024, **12**(12), 2851.
44 M. N. de Almeida, G. G. Halfeld, I. B. da Costa, L. G. de Lima Guimarães, B. Cordeiro and V. M. Guimarães, *Bioenergy Res.*, 2024, **17**, 281–293.
45 L. S. Oliveira and A. S. Franca, in *Coffee in Health and Disease Prevention*, ed. V. R. Preedy, Academic Press, San Diego, 2015, pp. 283–291.
46 R. P. Munirwan, A. Mohd Taib, M. R. Taha, N. Abd Rahman and M. Munirwansyah, *Physics and Chemistry of the Earth, Parts A/B/C*, 2022, **128**, 103252.
47 N. E. Torres Castillo, J. S. Ochoa Sierra, M. A. Oyervides-Muñoz, J. E. Sosa-Hernández, H. M. N. Iqbal, R. Parra-Saldívar and E. M. Melchor-Martínez, *Case Stud. Chem. Environ. Eng.*, 2021, **3**, 100070.
48 L. B. Cangussu, J. C. Melo, A. S. Franca and L. S. Oliveira, *Foods*, 2021, **10**(12), 3125.
49 W. J. Oosterkamp, in *Bioenergy Research: Advances and Applications*, ed. V. K. Gupta, M. G. Tuohy, C. P. Kubicek, J. Saddler and F. Xu, Elsevier, Amsterdam, 2014, pp. 203–217.
50 O. Oginni, K. Singh, G. Oporto, B. Dawson-Andoh, L. McDonald and E. Sabolsky, *Bioresour. Technol. Rep.*, 2019, **7**, 100266.
51 S. Brunauer, P. H. Emmett and E. Teller, *J. Am. Chem. Soc.*, 1938, **60**, 309–319.
52 A. I. Moral-Rodríguez, R. Leyva-Ramos, C. O. Ania, R. Ocampo-Pérez, E. D. Isaacs-Páez, D. H. Carrales-Alvarado and J. B. Parra, *Environ. Sci. Pollut. Res.*, 2019, **26**, 6141–6152.
53 N. Acelas, S. M. Lopera, J. Porras and R. A. Torres-Palma, *Molecules*, 2021, **26**(11), 3340.
54 M. Villen-Guzman, M. M. Cerrillo-Gonzalez, J. M. Paz-Garcia, J. M. Rodriguez-Maroto and B. Arhoun, *Environ. Technol. Innovation*, 2021, **21**, 101380.
55 N. Fairley, V. Fernandez, M. Richard-Plouet, C. Guillot-Deudon, J. Walton, E. Smith, D. Flahaut, M. Greiner, M. Biesinger, S. Tougaard, D. Morgan and J. Baltrusaitis, *Appl. Surf. Sci. Adv.*, 2021, **5**, 100112.
56 G. Limousin, J.-P. Gaudet, L. Charlet, S. Szenknect, V. Barthès and M. Krimissa, *Appl. Geochem.*, 2007, **22**, 249–275.
57 V. C. Srivastava, I. D. Mall and I. M. Mishra, *Chem. Eng. J.*, 2006, **117**, 79–91.
58 S. M. Khumalo, B. F. Bakare and S. Rathilal, *J. Hazard. Mater. Adv.*, 2024, **13**, 100404.
59 A. Forgionny, N. Y. Acelas, R. Ocampo-Pérez, E. Padilla-Ortega, S. Pérez and E. Flórez, *Environ. Nanotechnol., Monit. Manage.*, 2022, **18**, 100715.
60 H. C. Thomas, *J. Am. Chem. Soc.*, 1944, **66**, 1664–1666.
61 R. M. Clark, *Environ. Sci. Technol.*, 1987, **21**, 573–580.
62 E. A. Souza and L. A. Silva, *J. Environ. Chem. Eng.*, 2016, **4**, 2114–2120.
63 R. Ahmad and R. Kumar, *Appl. Surf. Sci.*, 2010, **257**, 1628–1633.
64 S. Meseldzija, J. Petrovic, A. Onjia, T. Volkov-Husovic, A. Nesic and N. Vukelic, *J. Ind. Eng. Chem.*, 2019, **75**, 246–252.
65 A. O. Egbedina, K. O. Adebowale, B. I. Olu-Owolabi, E. I. Unuabonah and M. O. Adesina, *RSC Adv.*, 2021, **11**, 18483–18492.
66 P. Liu, T. Song, R. Deng, X. Hou and J. Yi, *Environ. Sci. Pollut. Res.*, 2023, **30**, 53177–53190.
67 R. Li, Z. Wang, J. Guo, Y. Li, H. Zhang, J. Zhu and X. Xie, *Water Sci. Technol.*, 2018, **77**, 1127–1136.

68 P. S. Pauletto, S. F. Lütke, G. L. Dotto and N. P. G. Salau, *J. Mol. Liq.*, 2021, **336**, 116203.
69 S. Aguirre-Contreras, R. Leyva-Ramos, R. Ocampo-Pérez, C. G. Aguilar-Madera, J. V. Flores-Cano and N. A. Medellín-Castillo, *J. Water Process Eng.*, 2023, **54**, 103967.
70 V. Díaz-Blancas, C. G. Aguilar-Madera, J. V. Flores-Cano, R. Leyva-Ramos, E. Padilla-Ortega and R. Ocampo-Pérez, *J. Water Process Eng.*, 2020, **36**, 101303.
71 T. H. Tran, H. H. Le, T. H. Pham, D. T. Nguyen, D. D. La, S. W. Chang, S. M. Lee, W. J. Chung and D. D. Nguyen, *J. Environ. Chem. Eng.*, 2021, **9**, 105362.
72 F. Zapata, A. López-Fernández, F. Ortega-Ojeda, G. Quintanilla, C. García-Ruiz and G. Montalvo, *J. Chem. Educ.*, 2021, **98**, 2675–2686.
73 N. Przybylska, M. Śliwińska-Bartkowiak, M. Kościński, K. Rotnicki, M. Bartkowiak and S. Jurga, *J. Mol. Liq.*, 2021, **336**, 115938.
74 J. C. Serna-Carrizales, A. I. Zárate Guzmán, A. Forgionny, N. Acelas, S. Pérez, J. Muñoz-Saldaña and R. Ocampo-Perez, *Environ. Res.*, 2024, **250**, 118559.
75 A. B. Azzam, Y. A. Tokhy, F. M. El Dars and A. A. Younes, *J. Water Process Eng.*, 2022, **49**, 103006.